Video Prediction Transformers without Recurrence or Convolution

Yujin Tang[*] *tangyujin0275@gmail.com*
Shanghai Jiao Tong University
University of California, Merced

Lu Qi[†] *qqlu1992@gmail.com*
Wuhan University

Xiangtai Li *xiangtai94@gmail.com*
Nanyang Technological University

Chao Ma *chaoma99@gmail.com*
Shanghai Jiao Tong University

Ming-Hsuan Yang *minghsuanyang@gmail.com*
University of California, Merced

Reviewed on OpenReview: *https://openreview.net/forum?id=Afvhu9Id8m*

Abstract

Video prediction has witnessed the emergence of RNN-based models led by ConvLSTM, and CNN-based models led by SimVP. Following the significant success of ViT, recent works have integrated ViT into both RNN and CNN frameworks, achieving improved performance. While we appreciate these prior approaches, we raise a fundamental question: Is there a simpler yet more effective solution that can eliminate the high computational cost of RNNs while addressing the limited receptive fields and poor generalization of CNNs? How far can it go with a simple pure transformer model for video prediction? In this paper, we propose PredFormer, a framework entirely based on Gated Transformers. We provide a comprehensive analysis of 3D Attention in the context of video prediction. Extensive experiments demonstrate that PredFormer delivers state-of-the-art performance across four standard benchmarks. The significant improvements in both accuracy and efficiency highlight the potential of PredFormer as a strong baseline for real-world video prediction applications. The source code and trained models are released at `https://github.com/yyyujintang/PredFormer`.

1 Introduction

Video Prediction (Wang et al., 2018c; Chang et al., 2021; Gao et al., 2022a), also named as Spatio-Temporal predictive learning (Wang et al., 2017; 2018b; Tan et al., 2023a;b) involves learning spatial and temporal patterns by predicting future frames based on past observations. This capability is essential for various applications, including weather forecasting (Rasp et al., 2020; Pathak et al., 2022; Bi et al., 2023), traffic flow prediction (Fang et al., 2019; Wang et al., 2019), precipitation nowcasting (Shi et al., 2015; Gao et al., 2022b) and human motion forecasting (Zhang et al., 2017b; Wang et al., 2018a).

Despite the success of various video prediction methods, they often struggle to balance computational cost and performance. On the one hand, high-powered recurrent-based methods (Shi et al., 2015; Wang et al.,

[1]Project Page: `https://yyyujintang.github.io/predformer-project/` ; [*] Work done while visiting University of California, Merced. [†] Corresponding author.

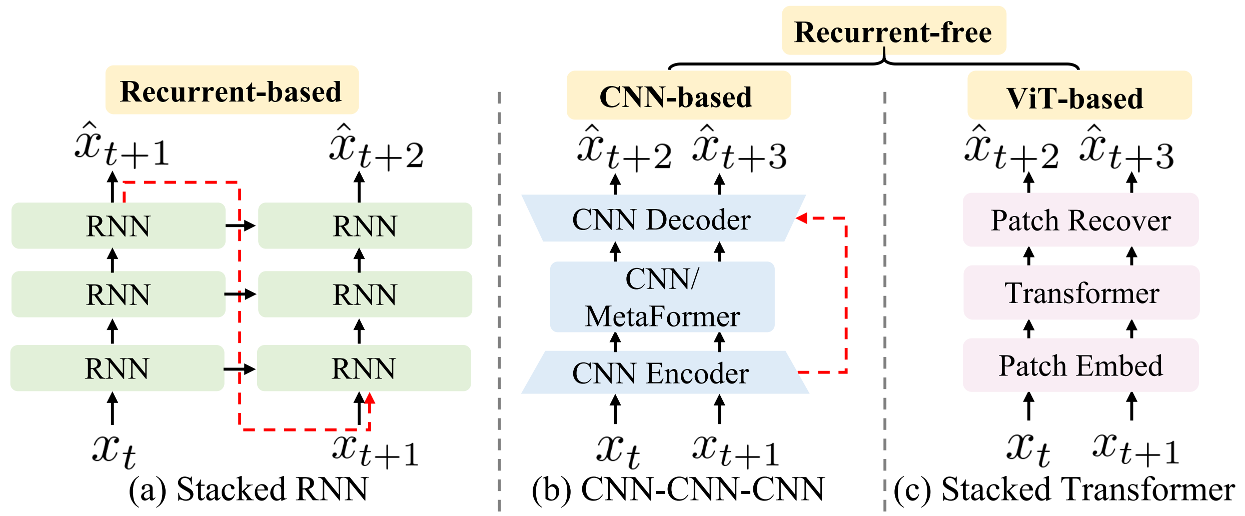

Figure 1: Main categories of video prediction framework. (a) Recurrent-based Framework (b) CNN Encoder-Decoder-based Recurrent-free Framework. (c) Pure transformer-based Recurrent-free Framework.

2017; 2019; Chang et al., 2021; Yu et al., 2019; Tang et al., 2023; 2024) rely heavily on autoregressive RNN frameworks, which face significant limitations in parallelization and computational efficiency. On the other hand, efficient recurrent-free methods (Gao et al., 2022a; Tan et al., 2023a), such as those based on the SimVP framework, use CNNs in an encoder-decoder architecture but are constrained by local receptive fields, limiting their scalability and generalization. The ensuing question is *Can we develop a framework that autonomously learns spatiotemporal dependencies without relying on inductive bias?*

An intuitive solution directly adopts a pure transformer (Vaswani et al., 2017) structure, as it is an efficient alternative to RNNs and has better scalability than CNNs. Transformers have demonstrated remarkable success in visual tasks (Dosovitskiy et al., 2020; Liu et al., 2021; Bertasius et al., 2021; Arnab et al., 2021; Tarasiou et al., 2023). Previous video prediction methods try to combine Swin Transformer (Liu et al., 2021) in recurrent-based frameworks such as SwinLSTM (Tang et al., 2023) and integrate MetaFormer (Yu et al., 2022) as a temporal translator in recurrent-free CNN-based encoder-decoder frameworks such as OpenSTL (Tan et al., 2023b). Despite these advances, pure transformer-based architecture remains underexplored mainly due to the challenges of capturing spatial and temporal relationships within a unified framework. While merging spatial and temporal dimensions and applying full attention is conceptually straightforward, it is computationally expensive because of the quadratic scaling of attention with sequence length. Several recent methods (Bertasius et al., 2021; Arnab et al., 2021; Tarasiou et al., 2023) decouple full attention and show that spatial and temporal relations can be treated separately in a factorized or interleaved manner to reduce complexity.

In this work, we propose PredFormer, a pure transformer-based architecture for video prediction. PredFormer dives into the decomposition of spatial and temporal transformers, integrating self-attention with gated linear units (Dauphin et al., 2017) to more effectively capture complex spatiotemporal dynamics. In addition to retaining spatial-temporal full attention encoder and factorized encoder strategies for both spatial-first and temporal-first configurations, we introduce six novel interleaved spatiotemporal transformer architectures, resulting in nine configurations. We explore how far this simple framework can go with different strategies of 3D Attention. This comprehensive investigation pushes the boundaries of current models and sets valuable benchmarks for spatial-temporal modeling.

Notably, PredFormer achieves state-of-the-art performance across four benchmark data sets, including synthetic prediction of moving objects, real-world human motion prediction, traffic flow prediction and weather forecasting, outperforming previous methods by a substantial margin without relying on complex model architectures or specialized loss functions.

The main contributions can be summarized as follows:

- We propose PredFormer, a pure gated transformer-based framework for video prediction. By eliminating the inductive biases inherent in CNNs, PredFormer harnesses the scalability and generalization capabilities of the transformers, achieving significantly enhanced performance ceilings with efficiency.
- We perform an in-depth analysis of spatial-temporal transformer factorization, exploring full-attention encoders and factorized encoders along with interleaved spatiotemporal transformer architectures, resulting in nine PredFormer variants. These variants address the differing spatial and temporal resolutions across tasks and datasets for optimal performance.
- We conduct a comprehensive study on training ViT from scratch on small datasets, exploring regularization and position encoding techniques.
- Extensive experiments demonstrate the state-of-the-art performance of PredFormer. It outperforms SimVP by 48% while achieving 1.5× faster inference speed on Moving MNIST. Besides, PredFormer surpasses SimVP with 8×, 5×, and 3× inference speed on TaxiBJ, WeatherBench, and Human3.6m, while achieving higher accuracy.

2 Related Work

Recurrent-based video prediction. Recent advancements in recurrent-based video prediction models have integrated CNNs, ViTs, and Vision Mamba (Liu et al., 2024) into RNNs, employing various strategies to capture spatiotemporal relationships. ConvLSTM (Shi et al., 2015), evolving from FC-LSTM (Srivastava et al., 2015), innovatively integrates convolutional operations into the LSTM framework. PredNet (Lotter et al., 2017) leverages deep recurrent convolutional neural networks with bottom-up and top-down connections to predict future video frames. PredRNN (Wang et al., 2017) introduces the Spatiotemporal LSTM (ST-LSTM) unit, which effectively captures and memorizes spatial and temporal representations by propagating hidden states horizontally and vertically. PredRNN++ (Wang et al., 2018b) incorporates a gradient highway unit and Causal LSTM to address the vanishing gradient problem and adaptively capture temporal dependencies. E3D-LSTM (Wang et al., 2018c) extends the memory capabilities of ST-LSTM by integrating 3D convolutions. The MIM model (Wang et al., 2019) further refines the ST-LSTM by reimagining the forget gate with dual recurrent units and utilizing differential information between hidden states. CrevNet (Yu et al., 2019) employs a CNN-based reversible architecture to decode complex spatiotemporal patterns. PredRNNv2 (Wang et al., 2022) enhances PredRNN by introducing a memory decoupling loss and a curriculum learning strategy. MAU (Chang et al., 2021) adds a motion-aware unit to capture dynamic motion information. SwinLSTM (Tang et al., 2023) integrates the Swin Transformer (Liu et al., 2021) module into the LSTM architecture, while VMRNN (Tang et al., 2024) extends this by incorporating the Vision Mamba module. Unlike these approaches, PredFormer is a recurrent-free method that offers superior efficiency.

Recurrent-free video prediction. Recent recurrent-free models, e.g., SimVP (Gao et al., 2022a), are developed based on a CNN-based encoder-decoder with a temporal translator. TAU (Tan et al., 2023a) builds upon this by separating temporal attention into static intra-frame and dynamic inter-frame components, introducing a differential divergence loss to supervise inter-frame variations. OpenSTL (Tan et al., 2023b) integrates a MetaFormer model as the temporal translator. Additionally, PhyDNet (Guen & Thome, 2020) incorporates physical principles into CNN architectures, while DMVFN (Hu et al., 2023) introduces a dynamic multi-scale voxel flow network to enhance video prediction performance. EarthFormer (Gao et al., 2022b) presents a 2D CNN encoder-decoder architecture with cuboid attention.WAST (Nie et al., 2024) proposes a wavelet-based method, coupled with a wavelet-domain High-Frequency Focal Loss. In contrast to prior methods, PredFormer advances video prediction with its recurrent-free, pure transformer-based architecture, leveraging a global receptive field to achieve superior performance, outperforming prior models without relying on complex architecture designs or specialized loss.

Recurrent-based approaches struggle with parallelization and performance, while CNN-based recurrent-free methods often sacrifice scalability and generalization despite their strong inductive biases. In contrast

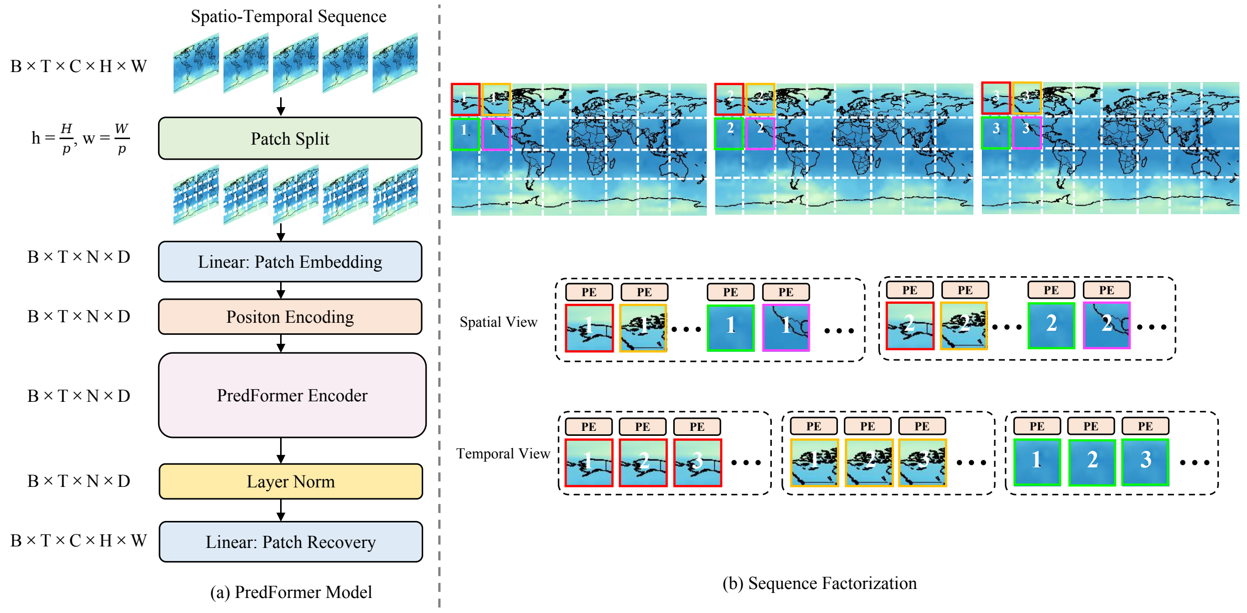

Figure 2: Overview of the PredFormer framework.

to prior methods, PredFormer advances video prediction with its recurrent-free, pure transformer-based architecture, leveraging a global receptive field to achieve superior performance, outperforming prior models without relying on complex model designs or specialized loss designs.

Vision Transformer (ViT). ViT (Dosovitskiy et al., 2020) has demonstrated exceptional performance on various vision tasks. In video processing, TimeSformer (Bertasius et al., 2021) investigates the factorization of spatial and temporal self-attention and proposes that divided attention where temporal and spatial attention are applied separately yields the best accuracy. ViViT (Arnab et al., 2021) explores factorized encoders, self-attention, and dot product mechanisms, concluding that a factorized encoder with spatial attention applied first performs better. On the other hand, TSViT (Tarasiou et al., 2023) finds that a factorized encoder prioritizing temporal attention achieves superior results. Latte (Ma et al., 2024) investigates factorized encoders and factorized self-attention mechanisms, incorporating both spatial-first and spatial-temporal parallel designs, within the context of latent diffusion transformers for video generation. Despite these advancements, most existing models focus primarily on video classification, with limited research on applying ViTs to spatio-temporal predictive learning. Moving beyond earlier methods that focus on factorizing self-attention, PredFormer explores the decomposition of spatial and temporal transformers at a deeper level by integrating self-attention with gated linear units and introducing innovative interleaved designs, allowing for a more robust capture of complex spatiotemporal dynamics.

3 Method

To systematically analyze the transformer structure of the network model in spatial-temporal predictive learning, we propose the PredFormer as a general model design, as shown in Fig 2. In the following sections, we introduce the pure transformer-based architecture in Sec 3.1. Next, we describe the Gated Transformer Block (GTB) in Sec 3.2. Finally, we present how to use GTB to build a PredFormer layer and architecture variants in Sec 3.3.

3.1 Pure Transformer Based Architecture

Patch Embedding. Follow the ViT design, PredFormer splits a sequence of frames $\mathcal{X}$ into a sequence of $N = \left\lfloor \frac{H}{p} \right\rfloor \left\lfloor \frac{W}{p} \right\rfloor$ equally sized, non-overlapping patches of size p, each of which is flattened into a 1D tokens.

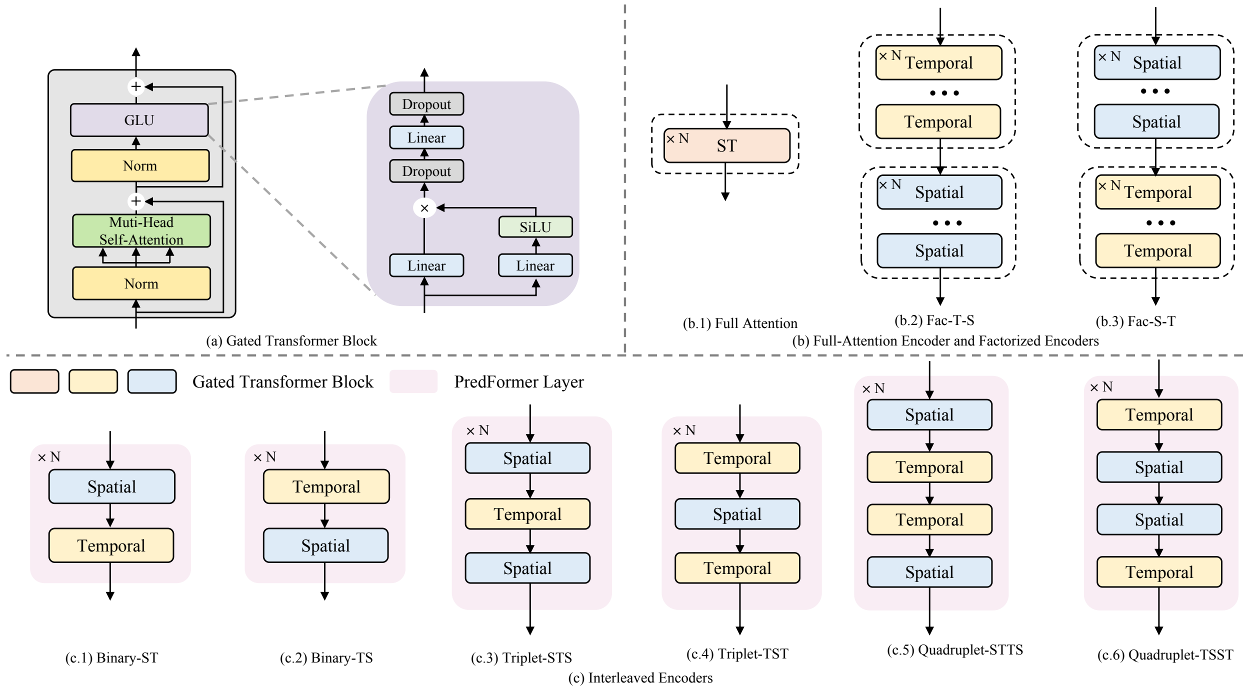

Figure 3: (a) Gated Transformer Block (b) Full Attention Encoder and Factorized Encoders (c) Interleaved Encoders with Binary, Triplet, and Quadrupled design

These tokens are then linearly projected into hidden dimensions D and processed by a layer normalization (LN) layer, resulting in a tensor $\mathcal{X}' \in \mathbb{R}^{B\times T\times N\times D}$.

Position Encoding. Unlike typical ViT approach, which employs learnable position embeddings, we incorporate a spatiotemporal position encoding (PE) generated by sinusoidal functions with absolute coordinates for each patch.

PredFormer Encoder. The 1D tokens are then processed by a PredFormer Encoder for feature extraction. PredFormer Encoder is stacked by Gated Transformer Blocks in various manners.

Patch Recovery. Since our encoder is based on a pure gated transformer, without convolution or resolution reduction, global context is modeled at every layer. This allows it to be paired with a simple decoder, forming a powerful prediction model. After the encoder, a linear layer serves as the decoder, projecting the hidden dimensions back to recover the 1D tokens to 2D patches.

3.2 Gated Transformer Block

The Standard Transformer model (Vaswani et al., 2017) alternates between Multi-Head Attention (MSA) and Feed-Forward Networks (FFN). The attention mechanism for each head is defined as:

$$\text{Attention}(\mathbf{Q},\mathbf{K},\mathbf{V}) = \text{Softmax}\left(\frac{\mathbf{Q}\mathbf{K}^\top}{\sqrt{d_k}}\right)\mathbf{V}, \tag{1}$$

where in self-attention, the queries $\mathbf{Q}$, keys $\mathbf{K}$, and values $\mathbf{V}$ are linear projections of the input $\mathbf{X}$, represented as $\mathbf{Q} = \mathbf{X}\mathbf{W}_q$, $\mathbf{K} = \mathbf{X}\mathbf{W}_k$, and $\mathbf{V} = \mathbf{X}\mathbf{W}_v$, with $\mathbf{X},\mathbf{Q},\mathbf{K},\mathbf{V} \in \mathbb{R}^{N\times d}$. The FFN then processes each position in the sequence by applying two linear transformations.

Gated Linear Units (GLUs) (Dauphin et al., 2017), often used in place of simple linear transformations, involve the element-wise product of two linear projections, with one projection passing through a sigmoid function. Various GLU variants control the flow of information by substituting the sigmoid with other non-linear functions. For instance, SwiGLU (Shazeer, 2020) replaces the sigmoid with the Swish activation

Table 1: Benchmark datasets used in our experiments. “Interval” denotes the temporal gap between two consecutive frames in the sequence (e.g., frame-level sampling, 30 minutes, or 1 hour).

Dataset	Training size	Testing size	Channel	Height	Width	Input T	Output T'	Interval
Moving MNIST	10,000	10,000	1	64	64	10	10	-
Human3.6m	73,404	8,582	3	256	256	4	4	frame
WeatherBench-S	52,559	17,495	1	32	64	12	12	30 min
TaxiBJ	20,461	500	2	32	32	4	4	1 hour

function (SiLU) (Hendrycks & Gimpel, 2016), as shown in Eq 2.

$$\begin{aligned}\mathrm{Swish}_\beta(x) &= x\sigma(\beta x)\\ \mathrm{SwiGLU}(x, W, V, b, c, \beta) &= \mathrm{Swish}_\beta(xW + b) \otimes (xV + c)\end{aligned} \tag{2}$$

SwiGLU has been demonstrated to outperform Multi-layer Perceptrons (MLPs) in various natural language processing tasks(Shazeer, 2020). Inspired by the SwiGLU’s success in these tasks, our Gated Transformer Block (GTB), incorporates MSA followed by a SwiGLU-based FFN, as illustrated in Fig 3(a). GTB is defined as:

$$\begin{aligned}\mathbf{Y}^l &= \mathrm{MSA}(\mathrm{LN}(\mathbf{Z}^l)) + \mathbf{Z}^l\\ \mathbf{Z}^{l+1} &= \mathrm{SwiGLU}(\mathrm{LN}(\mathbf{Y}^l)) + \mathbf{Y}^l\end{aligned} \tag{3}$$

3.3 Variants of PredFormer

Modeling spatiotemporal dependencies in video prediction is challenging, as the balance between spatial and temporal information differs significantly across tasks and datasets. Developing flexible and adaptive models that can accommodate varying dependencies and scales is thus critical. To address these, we explore both full-attention encoders and factorized encoders with spatial-first (Fac-S-T) and temporal-first (Fac-T-S) configurations, as shown in Fig 3(b). In addition, we introduce six interleaved models based on PredFormer layer, enabling dynamic interaction across multiple scales.

A PredFormer layer is a module capable of simultaneously processing spatial and temporal information. Building on this design principle, we propose three interleaved spatiotemporal paradigms, Binary, Triplet, and Quadruplet, which sequentially model the spatial and temporal views. Ultimately, they yield **six** distinct architectural configurations. A detailed illustration of these nine variants is provided in Fig 3.

For full attention layers, given input $\mathcal{X} \in \mathbb{R}^{B\times T\times N\times D}$, attention is computed over the sequence of length $T \times N$. As illustrated in Fig 3 (b.1), we merge and flatten the spatial and temporal tokens to compute attention through several stacked GTB_{st}.

For Binary layers, each GTB block processes temporal or spatial sequence independently, which we denote as a binary-TS or binary-ST layer. The input is first reshaped, and processed through GTB_t^1, where attention is applied over the temporal sequence. The tensor is then reshaped back to restore the temporal order. Subsequently, spatial attention is applied using another GTB_s^2, where the tensor is flattened along the temporal dimension and processed.

For Triplet and Quadruplet layers, additional blocks are stacked on top of the Binary structure. The Quadruplet layer combines two Binary layers in different orders.

4 Experiments

We present extensive evaluations of PredFormer and state-of-the-art methods. We conduct experiments across synthetic and real-world scenarios, including long-term prediction(moving object trajectory prediction and weather forecasting), and short-term prediction(traffic flow prediction and human motion prediction). The statistics of the data set are presented in the tab 1. These datasets have different spatial resolutions, temporal frames, and intervals, which determine their different spatiotemporal dependencies.

Table 2: Quantitative comparison on **Moving MNIST**. Each model observes 10 frames and predicts the subsequent 10 frames. We highlight the best experimental results in bold red and the second-best in blue.

Method	**Paras(M)**	**Flops(G)**	**FPS**	**Memory (MB)**	**MSE ↓**	**MAE ↓**	**SSIM ↑**
ConvLSTM	15.0	56.8	113	68.8	103.3	182.9	0.707
PredRNN	23.8	116.0	54	107.6	56.8	126.1	0.867
PredRNN++	38.6	171.7	38	164.1	46.5	106.8	0.898
MIM	38.0	179.2	37	160.6	44.2	101.1	0.910
E3D-LSTM	51.0	298.9	18	270.1	41.3	86.4	0.910
PhyDNet	3.1	15.3	182	149.5	24.4	70.3	0.947
MAU	4.5	17.8	201	35.4	27.6	86.5	0.937
PredRNNv2	24.6	708.0	24	109.0	48.4	129.8	0.891
SwinLSTM	20.2	69.9	62	96.4	17.7	-	0.962
SimVP	58.0	19.4	209	284.7	23.8	68.9	0.948
TAU	44.7	16.0	283	322.9	19.8	60.3	0.957
OpenSTL_ViT	46.1	16.9	290	331.8	19.0	60.8	0.955
OpenSTL_Swin	46.1	16.9	290	331.9	18.3	59.0	0.960
PredFormer							
Full Attention	25.3	21.2	254	135.9	17.3	56.0	0.962
Fac-S-T	25.3	16.5	368	117.4	20.6	63.5	0.955
Fac-T-S	25.3	16.5	370	117.4	16.9	55.8	0.963
Binary-TS	25.3	16.5	301	117.4	12.8	46.1	0.972
Binary-ST	25.3	16.5	316	117.4	13.4	47.1	0.971
Triplet-TST	25.3	16.4	312	118.0	13.4	47.2	0.971
Triplet-STS	25.3	16.5	321	118.0	13.1	46.7	0.972
Quadruplet-TSST	25.3	16.5	302	118.0	**12.4**	**44.6**	**0.973**
Quadruplet-STTS	25.3	16.4	322	118.0	**12.4**	44.9	**0.973**

Implementation Details Our method is implemented in PyTorch. The experiments were conducted on a single 24GB NVIDIA RTX 3090. PredFormer is optimized using the AdamW (Loshchilov & Hutter, 2019) optimizer with an L2 loss, a weight decay of 1e-2, and a learning rate selected from {5e-4, 1e-3} for best performance. OneCycle scheduler is used for Moving MNIST and TaxiBJ, while the Cosine scheduler is applied for Human3.6m and WeatherBench. Dropout (Hinton, 2012) and stochastic depth (Huang et al., 2016) regularization prevent overfitting. Further hyperparameter details are provided in the Appendix. For different PredFormer variants, we maintain a constant number of GTB blocks to ensure comparable parameters. In cases where the Triplet model cannot be evenly divided, we use the number of GTB blocks closest to the others.

Evaluation Metrics We assess model performance using a suite of metrics. (1) **Pixel-wise error** is measured using Mean Squared Error (MSE), Mean Absolute Error (MAE), and Root Mean Squared Error (RMSE). (2) **Predicted frame quality** is evaluated using the structural similarity index measure (SSIM) metric (Wang et al., 2004). Lower MSE, MAE, and RMSE values, combined with higher SSIM, signify better predictions. (3) **Computational efficiency** is assessed by the number of parameters, floating-point operations (FLOPs), and inference speed in frames per second (FPS) on a NVIDIA A6000 GPU. This evaluation framework comprehensively evaluates accuracy and efficiency.

4.1 Synthetic Moving Object Prediction

Moving MNIST. The moving MNIST dataset (Srivastava et al., 2015) serves as a benchmark synthetic dataset for evaluating sequence reconstruction models. We follow (Srivastava et al., 2015) to generate Moving MNIST sequences with 20 frames, using the initial 10 frames for input and the subsequent 10 frames as the prediction target. We adopt 10000 sequences for training, and for fair comparisons, we use the pre-generated 10000 sequences (Gao et al., 2022a) for validation.

On the Moving MNIST dataset, following prior work (Gao et al., 2022a; Tan et al., 2023a), we train our models for 2000 epochs and report our results in Tab 2. We train OpenSTL methods with ViT and Swin Transformer as temporal translators for 2000 epochs as recurrent-free baselines. We cite other results from each original paper for a fair comparison.

Compared to SimVP, PredFormer achieves substantial performance gains while maintaining a lightweight structure. Specifically, it reduces MSE by 48% (from 23.8 to 12.4), significantly improving prediction accu-

Table 3: Quantitative comparison on **Human3.6m**. Each model observes 4 frames and predicts the subsequent 4 frames.

Method	Paras(M)	Flops(G)	FPS	Memory(MB)	MSE ↓	MAE ↓	SSIM ↑	PSNR ↑	LPIPS ↓
ConvLSTM	15.5	347.0	52	142.7	125.5	1566.7	0.9813	33.40	0.03557
PredNet	12.5	13.7	176	120.8	261.9	1625.3	0.9786	31.76	0.03264
PredRNN	24.6	704.0	25	327.2	113.2	1458.3	0.9831	33.94	0.03245
PredRNN++	39.3	1033.0	18	402.3	**110.0**	1452.2	0.9832	34.02	0.03196
MIM	47.6	1051.0	17	434.8	112.1	1467.1	0.9829	33.97	0.03338
E3D-LSTM	60.9	542.0	7	548.9	143.3	1442.5	0.9803	32.52	0.04133
PhyDNet	4.2	19.1	57	67.9	125.7	1614.7	0.9804	33.05	0.03709
MAU	20.2	105.0	6	371.2	127.3	1577.0	0.9812	33.33	0.03561
PredRNNv2	24.6	708.0	24	350.5	114.9	1484.7	0.9827	33.84	0.03334
SimVP	41.2	197.0	26	556.4	115.8	1511.5	0.9822	33.73	0.03467
TAU	37.6	182.0	26	551.8	113.3	1390.7	**0.9839**	34.03	0.02783
OpenSTL_ViT	11.0	142.2	35	1170.0	136.3	1603.5	0.9796	33.10	0.03729
OpenSTL_Swin	38.8	188.0	28	562.3	133.2	1599.7	0.9799	33.16	0.03766
PredFormer									
Full Attention	12.7	155.0	16	1120.7	113.9	1412.4	0.9833	33.98	0.03279
Fac-S-T	12.7	65.0	76	352.7	153.4	1630.7	0.9784	32.30	0.04676
Fac-T-S	12.7	65.0	75	356.7	118.4	1504.7	0.9820	33.67	0.03284
Binary-TS	12.7	65.0	75	352.7	111.2	1380.4	0.9838	34.13	0.03008
Binary-ST	12.7	65.0	78	348.7	112.7	1386.3	0.9836	34.07	0.03017
Triplet-TST*	12.7	60.8	88	352.7	112.4	1406.2	0.9834	34.05	**0.02748**
Triplet-STS*	12.7	69.3	64	356.7	111.8	1410.3	0.9834	34.07	0.02933
Quadruplet-TSST	12.7	65.0	72	352.7	110.9	**1380.3**	**0.9839**	**34.14**	0.03069
Quadruplet-STTS	12.7	65.0	74	356.7	113.4	1405.7	0.9835	34.04	0.02918

For * models, we add a skip connection for each PredFormer Layer for stable training.

racy. Meanwhile, PredFormer requires far fewer parameters (25.3M vs. 58.0M in SimVP) and operates with lower FLOPs (16.5G vs. 19.4G), showcasing its superior efficiency.

Notably, even when SimVP incorporates ViT and Swin Transformer as the temporal translator, its performance remains far below that of PredFormer. This is because, while SimVP benefits from the inductive bias of using CNNs as the encoder and decoder, this design inherently limits the model's performance ceiling. In contrast, PredFormer effectively models global spatiotemporal dependencies, allowing it to surpass these constraints and achieve superior predictive accuracy.

Compared to SwinLSTM, PredFormer achieves higher accuracy. Although SwinLSTM outperforms SimVP in terms of MSE (17.7 vs. 23.8), its reliance on an RNN-based structure results in significantly higher computational cost. SwinLSTM exhibits high FLOPs (69.9G) and lower FPS, making it less efficient for large-scale deployment. This highlights the limitations of recurrent structures in video prediction, whereas PredFormer, with its recurrence-free framework, achieves both higher accuracy and superior efficiency.

Among the PredFormer variants, Quadruplet-TSST achieves the best MSE of 12.4, followed closely by Quadruplet-STTS. These results highlight PredFormer's ability to fully leverage global information fully, further validating its effectiveness in video prediction.

4.2 Real-world Human Motion Prediction

Human3.6m. The Human3.6M dataset (Ionescu et al., 2014) comprises 3.6 million unique human poses with their corresponding images, serving as a benchmark for motion prediction tasks. Human motion prediction is particularly challenging due to high resolution input and complex human movement dynamics. Following OpenSTL (Tan et al., 2023b), we downsample the dataset from 1000×1000×3 to 256×256×3. We use four observations to predict the next four frames.

PredFormer achieves SOTA on Human3.6M. Compared to SimVP, PredFormer Quadruplet-TSST reduces MSE from 115.8 to 110.9, significantly improving human motion prediction. At the same time, PredFormer requires only 12.7M parameters, much fewer than SimVP's 41.2M. Furthermore, its computational cost is only 65G FLOPs, less than one third of SimVP's 197G, while maintaining a higher inference speed.

PredFormer also substantially reduces the computational cost compared to PredRNN++. While PredRNN++ requires 1033G FLOPs, PredFormer Quadruplet-TSST achieves comparative MSE and superior MAE and SSIM using only one-tenth of the computation.

Table 4: Quantitative comparison on **TaxiBJ**. Each model observes 4 frames and predicts the subsequent 4 frames.

Method	**Paras(M)**	**Flops(G)**	**FPS**	**Memory(MB)**	**MSE ↓**	**MAE ↓**	**SSIM ↑**
ConvLSTM	15.0	20.7	815	67.0	0.485	17.7	0.978
PredRNN	23.7	42.4	416	105.5	0.464	16.9	0.977
PredRNN++	38.4	63.0	301	162.8	0.448	16.9	0.971
MIM	37.9	64.1	275	158.4	0.429	16.6	0.971
E3D-LSTM	51.0	98.2	60	240.5	0.432	16.9	0.979
PhyDNet	3.1	5.6	982	149.3	0.362	15.5	0.983
PredRNNv2	23.7	42.6	378	106.8	0.383	15.5	0.983
SwinLSTM	2.9	1.3	1425	22.0	0.303	15.0	0.984
SimVP	13.8	3.6	533	183.9	0.414	16.2	0.982
TAU	9.6	2.5	1268	175.0	0.344	15.6	0.983
OpenSTL_ViT	9.7	2.8	1301	174.8	0.317	15.2	0.984
OpenSTL_Swin	9.7	2.6	1506	274.3	0.313	15.1	0.985
PredFormer							
Full Attention	8.4	2.4	2438	42.3	0.316	14.6	0.985
Fac-S-T	8.4	2.2	3262	42.4	0.320	15.2	0.984
Fac-T-S	8.4	2.2	3224	42.4	0.283	14.4	0.985
Binary-TS	8.4	2.2	3192	42.4	0.286	14.6	0.985
Binary-ST	8.4	2.2	3172	42.4	**0.277**	**14.3**	**0.986**
Triplet-TST	6.3	1.6	4348	34.4	0.293	14.7	0.985
Triplet-STS	6.3	1.6	4249	34.4	**0.277**	**14.3**	**0.986**
Quadruplet-TSST	8.4	2.2	3230	42.4	0.284	14.4	**0.986**
Quadruplet-STTS	8.4	2.2	3259	42.4	0.293	14.6	0.985

Compared to OpenSTL-ViT and OpenSTL-Swin Transformer, which rely on ViT-based architectures but struggle with prediction accuracy, PredFormer utilizes the Transformer structures more effectively for video prediction. OpenSTL-ViT and OpenSTL-Swin both perform worse than SimVP, indicating that simply applying Transformers does not guarantee strong results. In contrast, PredFormer outperforms them while maintaining an efficient design, demonstrating its capability in spatiotemporal modeling.

4.3 Traffic Flow Prediction

TaxiBJ. TaxiBJ (Zhang et al., 2017a) includes GPS data from taxis and meteorological data in Beijing. Each data frame is visualized as a $32 \times 32 \times 2$ heatmap, where the third dimension encapsulates the inflow and outflow of traffic within a designated area. Following previous work (Zhang et al., 2017a), we allocate the final four weeks' data for testing, utilizing the preceding data for training. Our prediction model uses four sequential observations to forecast the subsequent four frames.

PredFormer achieves SOTA on TaxiBJ. Compared to SimVP, PredFormer significantly improves the accuracy of the prediction, reducing the MSE from 0.414 to 0.277 (33%) while using fewer parameters (8.4M vs 13.8M) and a lower computational cost (2.2G FLOPs vs. 3.6G FLOPs). Despite this efficiency, PredFormer also dramatically increases inference speed, with FPS rising from 533 in SimVP to 4249.

Furthermore, OpenSTL-ViT and OpenSTL-Swin, which adopt ViT-based architectures as temporal translators, achieve MSEs of 0.317 and 0.313, both worse than PredFormer's best results. This suggests that using CNNs for the encoder and decoder provides a strong inductive bias but inherently limits the model's performance. Among the variants of PredFormer, Binary-ST and Triplet-STS achieve the best MSE of 0.277.

4.4 Weather Forecasting

WeatherBench. Climate prediction is a critical challenge in spatiotemporal predictive learning. The WeatherBench (Rasp et al., 2020) dataset provides a comprehensive global weather forecasting resource, covering various climatic factors. In our experiments, we utilize *WeatherBench-S*, a single-variable setup where each climatic factor is trained independently. We focus on temperature prediction at a 5.625° resolution (32×64 grid points). The model is trained on data spanning 2010-2015, validated on data from 2016, and tested on data from 2017-2018, all with a one-hour temporal interval. We input the first 12 frames and predict the subsequent 12 frames in this setting.

Table 5: Quantitative comparison on **WeatherBench(T2m)**. Each model observes 12 frames and predicts the subsequent 12 frames.

Method	**Paras(M)**	**Flops(G)**	**FPS**	**Memory(MB)**	**MSE ↓**	**MAE ↓**	**SSIM ↑**
ConvLSTM	14.9	136.0	46	69.8	1.521	0.7949	1.233
PredRNN	23.6	278.0	22	108.2	1.331	0.7246	1.154
PredRNN++	38.3	413.0	15	165.5	1.634	0.7883	1.278
MIM	37.8	109.0	126	275.9	1.784	0.8716	1.336
PhyDNet	3.1	36.8	177	150.6	285.9	8.7370	16.91
MAU	5.5	39.6	237	56.2	1.251	0.7036	1.119
PredRNNv2	23.6	279.0	22	110.8	1.545	0.7986	1.243
SimVP	14.8	8.0	196	194.7	1.238	0.7037	1.113
TAU	12.2	6.7	229	195.6	1.162	0.6707	1.078
OpenSTL_ViT	12.4	8.0	432	194.9	1.146	0.6712	1.070
OpenSTL_Swin	12.4	6.9	581	195.1	1.143	0.6735	1.069
PredFormer							
Full Attention	5.3	17.8	177	185.4	1.126	0.6540	1.061
Fac-S-T	5.3	8.5	888	53.9	1.783	0.8688	1.335
Fac-T-S	5.3	8.5	860	54.9	**1.100**	**0.6469**	**1.049**
Binary-TS	5.3	8.6	837	53.9	1.115	0.6508	1.056
Binary-ST	5.3	8.6	847	51.9	1.140	0.6571	1.068
Triplet-TST	4.0	6.3	1064	48.9	1.108	0.6492	1.053
Triplet-STS	4.0	6.5	1001	49.9	1.149	0.6658	1.072
Quadruplet-TSST	5.3	8.6	802	53.9	1.116	0.6510	1.057
Quadruplet-STTS	5.3	8.6	858	54.9	1.118	0.6507	1.057

Table 6: Ablation on PredFormer Layer Number on Moving MNIST.

TSST Layer	**Paras(M)**	**Flops(G)**	**FPS**	**MSE ↓**	**MAE ↓**	**SSIM ↑**
2	8.5	5.5	887	20.1	65.2	0.955
3	12.7	8.3	621	16.2	55.1	0.965
4	16.9	11.0	457	13.5	47.9	0.970
5	21.1	13.7	376	12.7	45.5	0.972
6	25.3	16.5	302	12.4	44.6	0.973
7	29.5	19.2	277	12.3	44.2	0.973
8	33.7	22.0	240	**11.7**	**41.8**	**0.975**

On WeatherBench (T2m), RNN-based models like ConvLSTM and PredRNN have high computational costs but poor performance. PredRNN and PredRNNv2 reach 278.0G and 279.0G FLOPs, yet their MSE remains at 1.331 and 1.545, respectively, highlighting the inefficiency of RNN structures for this task.

SimVP reduces parameter count to half of PredRNN, lowers FLOPs to 8.0G, and achieves an improved MSE of 1.238, making it more efficient than RNN models. PredFormer further improves performance, using only half the parameters of SimVP while maintaining similar or lower FLOPs, achieving the best MSE of 1.100. The Fac-T-S and Triplet-TST variants deliver the top results. It also demonstrates a significant FPS advantage, with Binary-TS and Triplet-TST achieving 837 and 1064 FPS, respectively, compared to SimVP's 196, highlighting the model's superior efficiency in both computation and prediction speed.

4.5 Ablation Study and Discussion

PredFormer Layer Number. We conduct an ablation study on the number of TSST layers in PredFormer to evaluate its scalability and potential for performance improvement, as shown in Tab 6. The results show that as the number of layers increases, PredFormer continues to achieve better results, surpassing the 6-layer TSST configuration reported in Tab 2. With 2 TSST layers, PredFormer already outperforms SimVP, achieving a lower MSE of 20.1 while maintaining high efficiency. When increasing to 3 layers, PredFormer surpasses TAU, OpenSTL-ViT, and OpenSTL-Swin, achieving a lower MSE of 16.2 while requiring only half the FLOPs of these models and delivering twice their FPS. With 8 layers, PredFormer achieves an MSE of 11.7, which represents a 51% MSE reduction compared to SimVP. This substantial improvement demonstrates the scalability of PredFormer.

We conduct ablation studies on PredFormer model design and summarize the results in Tab 7 and Tab 8. We choose the best Triplet-STS model on TaxiBJ, and the best Fac-T-S model on WeatherBench as baselines.

Table 7: Ablation on Gate Linear Unit and Position Encoding.

	WeatherBench (T2m)			TaxiBJ	
Model	**MSE ↓**	**MAE ↓**	**RMSE ↓**	**MSE ↓**	**MAE ↓**
PredFormer	**1.100**	**0.6489**	**1.049**	**0.277**	**14.3**
SwiGLU → MLP	1.171	0.6707	1.082	0.306	15.1
PE: Abs → Learnable	1.164	0.6771	1.079	0.288	14.6

Table 8: Ablation on Dropout and Stochastic Depth.

	WeatherBench (T2m)			TaxiBJ	
Model	**MSE ↓**	**MAE ↓**	**RMSE ↓**	**MSE ↓**	**MAE ↓**
+ DP + Uni SD	**1.100**	**0.6489**	**1.049**	**0.277**	**14.3**
W/o Reg	1.244	0.7057	1.115	0.319	15.1
+ DP	1.210	0.6887	1.100	0.283	14.5
+ Uni SD	1.156	0.6573	1.075	0.288	14.6
+ DP + Linear SD	1.138	0.6533	1.067	0.299	14.8

Gate Linear Unit. Replacing SwiGLU with a standard MLP results in a notable performance degradation. On TaxiBJ, the MSE rises from 0.277 to 0.306, and on WeatherBench from 1.100 to 1.171. This consistent performance degradation highlights the critical role of the gating mechanism in modeling complex spatiotemporal dynamics.

Position Encoding. Additionally, the performance deteriorates when we replace the absolute positional encoding in our model with the learnable spatiotemporal encoding commonly used in ViT. On Moving TaxiBJ, the MSE rises from 0.277 to 0.288, and on WeatherBench from 1.100 to 1.164. These ablation experiments consistently reveal similar trends across all three datasets, emphasizing the robustness of our Position Encoding designs.

Model Regularization. Pure transformer architectures like ViT generally require large datasets for effective training, and overfitting can become challenging when applied to smaller datasets. In our experiments, overfitting is noticeable on WeatherBench and TaxiBJ. We experiment with different regularization techniques in Tab 8 and find that both dropout(DP) and stochastic depth (SD) individually improve performance compared to no regularization. However, the combination of the two provides the best results. Unlike conventional ViT practices, which use a linearly scaled drop path rate across different depths, a uniform drop path rate performs significantly better for our tasks.

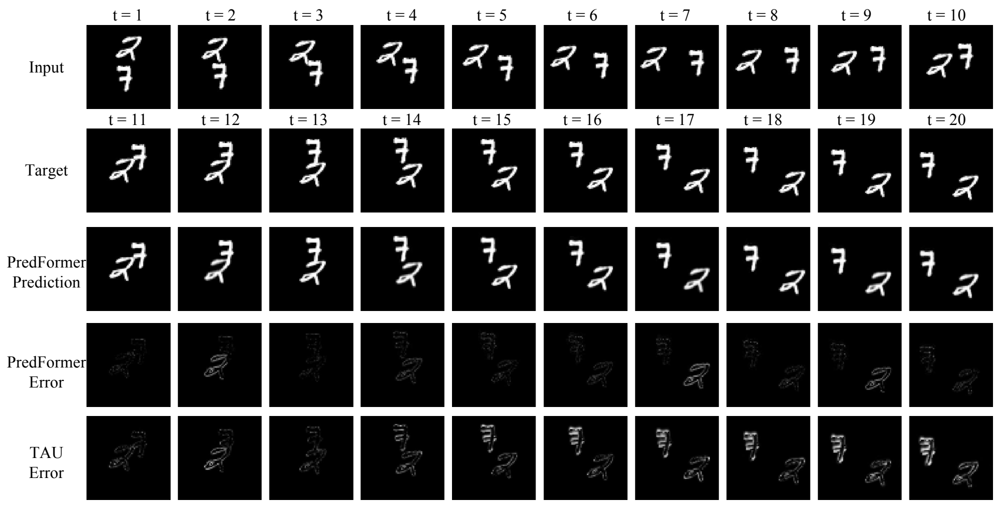

Figure 4: Visualizations on Moving MNIST. Error = |Prediction − Target|. We amplify the error for better comparison.

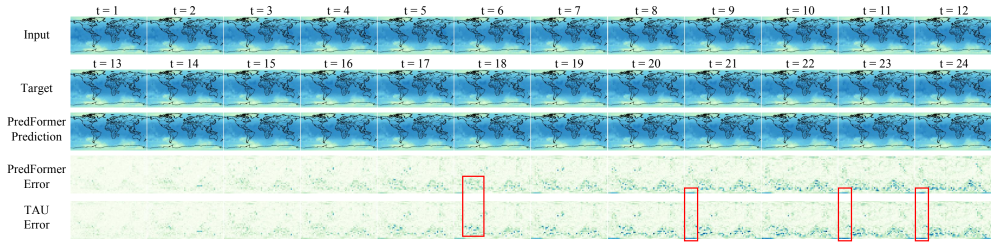

Figure 5: Visualizations on WeatherBench for global temperature forecasting.

Visualization. Fig 4, 5 and 6 provide a visual comparison of PredFormer's prediction results and prediction errors with Ground Truth. For Moving MNIST, our model accurately captures digit trajectories, with significantly lower accumulated error compared to TAU. On TaxiBJ, PredFormer effectively reconstructs the intricate spatial structures of traffic patterns, reducing high-frequency noise present in TAU's predictions. On WeatherBench, PredFormer achieves sharper and more precise temperature forecasts, with error heatmaps showing lower deviations in critical regions. Lastly, for Human3.6m, PredFormer consistently preserves fine-grained motion details, demonstrating superior temporal coherence in video prediction. Additional visualizations are provided in the supplementary material.

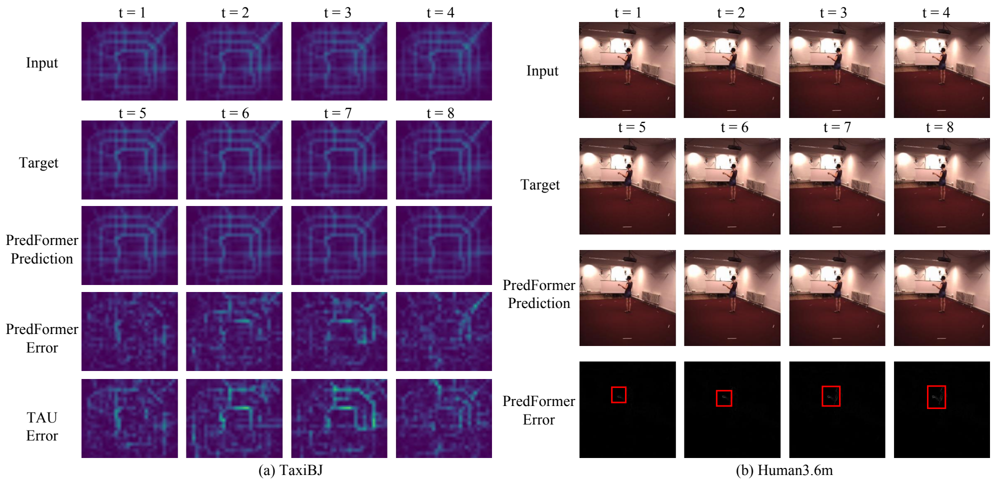

Figure 6: Visualizations on TaxiBJ and Human3.6m.

Discussion for PredFormer Variants. Despite our in-depth analysis of the spatiotemporal decomposition, the optimal model is not definite due to the different spatiotemporal dependent properties of the datasets. We recommend starting with the Quadruplet-TSST model for diverse video prediction tasks, which consistently performs well across datasets and configurations. Use M Quadruplet-TSST layers and experiment with models having a total of 4M GTBs to identify the optimal configuration. Then, explore Triplet-TST and Triplet-STS with M layers to find spatial and temporal dependencies. Unlike the SimVP framework, which adjusts hidden dimensions and block numbers separately for spatial encoder-decoder and temporal translator, PredFormer uses fixed hyperparameters for spatial and temporal GTBs, leveraging the scalability of the Transformer architecture. By simply adjusting the number of PredFormer layers, optimal results can be achieved with minimal tuning. We provide further theoretical analysis in the Appendix.

5 Conclusion

In this paper, we introduce PredFormer, a pure Transformer-based framework for video prediction, and systematically study how different spatio-temporal factorization patterns affect efficiency and accuracy. Across four standard benchmarks, PredFormer achieves strong performance while maintaining favorable

FLOPs, FPS, and memory usage compared to prior CNN- and RNN-based models, providing a competitive recurrent-free and convolution-free alternative. On the four benchmarks we study, our experiments suggest several dataset-dependent tendencies: interleaved spatio-temporal architectures generally offer the best balance between cost and accuracy; temporal-first factorizations often work particularly well for long-horizon forecasting, while other interleaved patterns can be preferable when the spatial structure is richer or the horizon is shorter; combining dropout with uniform stochastic depth is especially effective on overfitting-prone datasets; and absolute positional encoding is consistently more robust than learnable alternatives.

References

Anurag Arnab, Mostafa Dehghani, Georg Heigold, Chen Sun, Mario Lučić, and Cordelia Schmid. Vivit: A video vision transformer. In *ICCV*, 2021.

Gedas Bertasius, Heng Wang, and Lorenzo Torresani. Is space-time attention all you need for video understanding? In *ICML*, 2021.

Kaifeng Bi, Lingxi Xie, Hengheng Zhang, Xin Chen, Xiaotao Gu, and Qi Tian. Accurate medium-range global weather forecasting with 3d neural networks. In *Nature*, 2023.

Zheng Chang, Xinfeng Zhang, Shanshe Wang, Siwei Ma, Yan Ye, Xiang Xinguang, and Wen Gao. Mau: A motion-aware unit for video prediction and beyond. In *NeurIPS*, 2021.

Yann N Dauphin, Angela Fan, Michael Auli, and David Grangier. Language modeling with gated convolutional networks. In *ICML*, 2017.

Alexey Dosovitskiy, Lucas Beyer, Alexander Kolesnikov, Dirk Weissenborn, Xiaohua Zhai, Thomas Unterthiner, Mostafa Dehghani, Matthias Minderer, Georg Heigold, Sylvain Gelly, et al. An image is worth 16x16 words: Transformers for image recognition at scale. In *ICLR*, 2020.

Shen Fang, Qi Zhang, Gaofeng Meng, Shiming Xiang, and Chunhong Pan. Gstnet: Global spatial-temporal network for traffic flow prediction. In *IJCAI*, 2019.

Zhangyang Gao, Cheng Tan, Lirong Wu, and Stan Z Li. Simvp: Simpler yet better video prediction. In *CVPR*, 2022a.

Zhihan Gao, Xingjian Shi, Hao Wang, Yi Zhu, Yuyang Bernie Wang, Mu Li, and Dit-Yan Yeung. Earthformer: Exploring space-time transformers for earth system forecasting. In *NeurIPS*, 2022b.

Vincent Le Guen and Nicolas Thome. Disentangling physical dynamics from unknown factors for unsupervised video prediction. In *CVPR*, 2020.

Dan Hendrycks and Kevin Gimpel. Gaussian error linear units (gelus). In *Arxiv*, 2016.

GE Hinton. Improving neural networks by preventing co-adaptation of feature detectors. In *Arxiv*, 2012.

Xiaotao Hu, Zhewei Huang, Ailin Huang, Jun Xu, and Shuchang Zhou. A dynamic multi-scale voxel flow network for video prediction. In *CVPR*, 2023.

Gao Huang, Yu Sun, Zhuang Liu, Daniel Sedra, and Kilian Q Weinberger. Deep networks with stochastic depth. In *ECCV*, 2016.

Catalin Ionescu, Dragos Papava, Vlad Olaru, and Cristian Sminchisescu. Human3.6m: Large scale datasets and predictive methods for 3d human sensing in natural environments. In *TPAMI*, 2014.

Yue Liu, Yunjie Tian, Yuzhong Zhao, Hongtian Yu, Lingxi Xie, Yaowei Wang, Qixiang Ye, and Yunfan Liu. Vmamba: Visual state space model. In *Arxiv*, 2024.

Ze Liu, Yutong Lin, Yue Cao, Han Hu, Yixuan Wei, Zheng Zhang, Stephen Lin, and Baining Guo. Swin transformer: Hierarchical vision transformer using shifted windows. In *ICCV*, 2021.

Ilya Loshchilov and Frank Hutter. Decoupled weight decay regularization. In *ICLR*, 2019.

William Lotter, Gabriel Kreiman, and David Cox. Deep predictive coding networks for video prediction and unsupervised learning. In *ICLR*, 2017.

Xin Ma, Yaohui Wang, Gengyun Jia, Xinyuan Chen, Ziwei Liu, Yuan-Fang Li, Cunjian Chen, and Yu Qiao. Latte: Latent diffusion transformer for video generation. In *Arxiv*, 2024.

Xuesong Nie, Yunfeng Yan, Siyuan Li, Cheng Tan, Xi Chen, Haoyuan Jin, Zhihang Zhu, Stan Z Li, and Donglian Qi. Wavelet-driven spatiotemporal predictive learning: Bridging frequency and time variations. In *AAAI*, 2024.

Jaideep Pathak, Shashank Subramanian, Peter Harrington, Sanjeev Raja, Ashesh Chattopadhyay, Morteza Mardani, Thorsten Kurth, David Hall, Zongyi Li, Kamyar Azizzadenesheli, et al. Fourcastnet: A global data-driven high-resolution weather model using adaptive fourier neural operators. In *Arxiv*, 2022.

Stephan Rasp, Peter D Dueben, Sebastian Scher, Jonathan A Weyn, Soukayna Mouatadid, and Nils Thuerey. Weatherbench: a benchmark data set for data-driven weather forecasting. In *Journal of Advances in Modeling Earth Systems*, 2020.

Noam Shazeer. Glu variants improve transformer. In *Arxiv*, 2020.

Xingjian Shi, Zhourong Chen, Hao Wang, Dit-Yan Yeung, Wai-Kin Wong, and Wang-chun Woo. Convolutional lstm network: A machine learning approach for precipitation nowcasting. In *NeurIPS*, 2015.

Nitish Srivastava, Elman Mansimov, and Ruslan Salakhudinov. Unsupervised learning of video representations using lstms. In *ICML*, 2015.

Cheng Tan, Zhangyang Gao, Lirong Wu, Yongjie Xu, Jun Xia, Siyuan Li, and Stan Z Li. Temporal attention unit: Towards efficient spatiotemporal predictive learning. In *CVPR*, 2023a.

Cheng Tan, Siyuan Li, Zhangyang Gao, Wenfei Guan, Zedong Wang, Zicheng Liu, Lirong Wu, and Stan Z Li. Openstl: A comprehensive benchmark of spatio-temporal predictive learning. In *NeurIPS*, 2023b.

Song Tang, Chuang Li, Pu Zhang, and RongNian Tang. Swinlstm: Improving spatiotemporal prediction accuracy using swin transformer and lstm. In *ICCV*, 2023.

Yujin Tang, Peijie Dong, Zhenheng Tang, Xiaowen Chu, and Junwei Liang. Vmrnn: Integrating vision mamba and lstm for efficient and accurate spatiotemporal forecasting. In *CVPRW*, 2024.

Michail Tarasiou, Erik Chavez, and Stefanos Zafeiriou. Vits for sits: Vision transformers for satellite image time series. In *CVPR*, 2023.

Ashish Vaswani, Noam Shazeer, Niki Parmar, Jakob Uszkoreit, Llion Jones, Aidan N Gomez, Łukasz Kaiser, and Illia Polosukhin. Attention is all you need. In *NeurIPS*, 2017.

Pichao Wang, Wanqing Li, Philip Ogunbona, Jun Wan, and Sergio Escalera. Rgb-d-based human motion recognition with deep learning: A survey. In *Computer Vision and Image Understanding*, 2018a.

Yunbo Wang, Mingsheng Long, Jianmin Wang, Zhifeng Gao, and Philip S Yu. Predrnn: Recurrent neural networks for predictive learning using spatiotemporal lstms. In *NeurIPS*, 2017.

Yunbo Wang, Zhifeng Gao, Mingsheng Long, Jianmin Wang, and S Yu Philip. Predrnn++: Towards a resolution of the deep-in-time dilemma in spatiotemporal predictive learning. In *ICML*, 2018b.

Yunbo Wang, Lu Jiang, Ming-Hsuan Yang, Li-Jia Li, Mingsheng Long, and Li Fei-Fei. Eidetic 3d lstm: A model for video prediction and beyond. In *ICLR*, 2018c.

Yunbo Wang, Jianjin Zhang, Hongyu Zhu, Mingsheng Long, Jianmin Wang, and Philip S Yu. Memory in memory: A predictive neural network for learning higher-order non-stationarity from spatiotemporal dynamics. In *CVPR*, 2019.

Yunbo Wang, Haixu Wu, Jianjin Zhang, Zhifeng Gao, Jianmin Wang, S Yu Philip, and Mingsheng Long. Predrnn: A recurrent neural network for spatiotemporal predictive learning. In *TPAMI*, 2022.

Zhou Wang, Alan C Bovik, Hamid R Sheikh, and Eero P Simoncelli. Image quality assessment: from error visibility to structural similarity. In *TIP*, 2004.

Wei Yu, Yichao Lu, Steve Easterbrook, and Sanja Fidler. Efficient and information-preserving future frame prediction and beyond. In *ICLR*, 2019.

Weihao Yu, Mi Luo, Pan Zhou, Chenyang Si, Yichen Zhou, Xinchao Wang, Jiashi Feng, and Shuicheng Yan. Metaformer is actually what you need for vision. In *CVPR*, 2022.

Junbo Zhang, Yu Zheng, and Dekang Qi. Deep spatio-temporal residual networks for citywide crowd flows prediction. In *AAAI*, 2017a.

Liang Zhang, Guangming Zhu, Peiyi Shen, Juan Song, Syed Afaq Shah, and Mohammed Bennamoun. Learning spatiotemporal features using 3dcnn and convolutional lstm for gesture recognition. In *ICCVW*, 2017b.

A Appendix

A.1 Problem Definition

Video prediction is to learn spatial and temporal patterns by predicting future frames based on past observations. Given a sequence of frames $\mathcal{X}^{t:T} = \{\boldsymbol{x}^i\}_{t-T+1}^{t}$, which encapsulates the last T frames leading up to time t, the goal is to forecast the following T' frames $\mathcal{Y}^{t+1:T'} = \{\boldsymbol{x}^i\}_{t+1}^{t+1+T'}$ starting from time $t+1$. The input and the output sequence are represented as tensors $\mathcal{X}^{t:T} \in \mathbb{R}^{T \times C \times H \times W}$ and $\mathcal{Y}^{t+1:T'} \in \mathbb{R}^{T' \times C \times H \times W}$, where C, H, and W denote channel, height, and width of frames, respectively. The T and T' are the input and output frame numbers. For brevity, we use $\mathcal{X}$ and $\mathcal{Y}$ to denote $\mathcal{X}^{t:T}$ and $\mathcal{Y}^{t+1:T'}$ in the following sections.

Generally, we adopt a deep model equipped with learnable parameters $\mathcal{F}_\Theta$ for future frame prediction. The optimal set of parameters Θ^* is obtained by solving the optimization problem:

$$\Theta^* = \arg\min_{\Theta} \mathcal{L}(\mathcal{F}_\Theta(\mathcal{X}), \mathcal{Y}) \tag{4}$$

where $\mathcal{L}$ is the loss function measuring the difference between the prediction and the ground truth.

A.2 Data Transform

We provide a detailed description of the data transformation with PredFormer Binary-ST Layer in Eq 5. The data transformations for other variants follow a similar process.

$$\begin{aligned}
[B,T,N,D] \rightarrow [B*T,N,D], x_s &= \mathrm{GTB}_s^1(x_s.\mathrm{flatten}(0,1)) \\
[B*T,N,D] \rightarrow [B,N,T,D], x_s &= x_s.\mathrm{reshape}(B,T,N,D).\mathrm{T}(1,2) \\
[B,N,T,D] \rightarrow [B*N,T,D], x_{st} &= \mathrm{GTB}_t^2(x_s.\mathrm{flatten}(0,1)) \\
[B*N,T,D] \rightarrow [B,T,N,D], x_{st} &= x_{st}.\mathrm{reshape}(B,N,T,D).\mathrm{T}(1,2)
\end{aligned} \tag{5}$$

A.3 Theoretical Complexity Analysis

Setup and notation. We provide a formal complexity analysis of the nine PredFormer variants in terms of the temporal length T, the number of spatial patches N, and the hidden dimension D. For a fair comparison, all variants are instantiated under the same overall attention budget: we fix the depth of the network (the number of spatio-temporal blocks) and only change how the self-attention operations inside each block are allocated along the temporal and spatial dimensions. In other words, the total number of self-attention blocks is kept comparable across variants, and the differences in complexity come from the factorization pattern, rather than from simply increasing the number of layers.

Temporal vs. spatial self-attention. Let a temporal self-attention block operate on N independent sequences of length T (one for each spatial patch), and a spatial self-attention block operate on T independent sequences of length N (one for each time step). Ignoring constant factors and linear projections, the dominant terms are:

- **Temporal self-attention** over sequences of length T:

$$\text{Compute} \sim \mathcal{O}(T^2 N D), \qquad \text{Memory} \sim \mathcal{O}(T^2 N).$$

- **Spatial self-attention** over N patches:

$$\text{Compute} \sim \mathcal{O}(T N^2 D), \qquad \text{Memory} \sim \mathcal{O}(T N^2).$$

- **Full spatio-temporal self-attention** over all TN tokens:

$$\text{Compute} \sim \mathcal{O}\big((TN)^2 D\big), \qquad \text{Memory} \sim \mathcal{O}\big((TN)^2\big).$$

Table 9: Theoretical per-unit compute and memory complexity of the nine PredFormer variants and representative CNN/RNN baselines. For PredFormer, T is the temporal length, N is the number of spatial *patch* tokens (i.e., $N = HW/P^2$ for patch size P), and D is the hidden dimension. For convolutional and recurrent baselines, we instead use the spatial grid size $H \cdot W$ (pixels or grid cells) to denote the number of spatial locations. c_t and c_s denote the number of temporal and spatial self-attention blocks in one spatio-temporal unit, and c_j denotes the number of joint spatio-temporal attention blocks. We report only the leading terms and omit constant factors and lower-order terms.

Variant / Baseline	(c_t, c_s, c_j)	Compute Complexity	Memory Complexity
PredFormer variants (patch tokens N)			
Full Attention	$(0,0,1)$	$\mathcal{O}\big((TN)^2D\big)$	$\mathcal{O}\big((TN)^2\big)$
Fac-S-T	$(1,1,0)$	$\mathcal{O}\big(TN^2D + T^2ND\big)$	$\mathcal{O}\big(TN^2 + T^2N\big)$
Fac-T-S	$(1,1,0)$	$\mathcal{O}\big(TN^2D + T^2ND\big)$	$\mathcal{O}\big(TN^2 + T^2N\big)$
Binary-TS	$(1,1,0)$	$\mathcal{O}\big(TN^2D + T^2ND\big)$	$\mathcal{O}\big(TN^2 + T^2N\big)$
Binary-ST	$(1,1,0)$	$\mathcal{O}\big(TN^2D + T^2ND\big)$	$\mathcal{O}\big(TN^2 + T^2N\big)$
Triplet-TST	$(2,1,0)$	$\mathcal{O}\big((2T^2N + TN^2)D\big)$	$\mathcal{O}\big(2T^2N + TN^2\big)$
Triplet-STS	$(1,2,0)$	$\mathcal{O}\big((T^2N + 2TN^2)D\big)$	$\mathcal{O}\big(T^2N + 2TN^2\big)$
Quadruplet-TSST	$(2,2,0)$	$\mathcal{O}\big((2T^2N + 2TN^2)D\big)$	$\mathcal{O}\big(2T^2N + 2TN^2\big)$
Quadruplet-STTS	$(2,2,0)$	$\mathcal{O}\big((2T^2N + 2TN^2)D\big)$	$\mathcal{O}\big(2T^2N + 2TN^2\big)$
Recurrent-based baselines (spatial grid $H \cdot W$)			
ConvLSTM / PredRNN-family	–	$\mathcal{O}\big(T(HW)D^2\big)$	$\mathcal{O}\big((HW)D\big)$
CNN-based baselines (spatial grid $H \cdot W$)			
SimVP-family	–	$\mathcal{O}\big(T(HW)D^2\big)$	$\mathcal{O}\big(T(HW)D\big)$

Let c_t and c_s denote the number of temporal and spatial self-attention blocks in one spatio-temporal unit (macro-block), respectively. For the Full Attention baseline, we denote by c_j the number of joint spatio-temporal attention blocks. The per-unit complexity of a factorized variant is then given by:

$$\text{Compute} \sim \mathcal{O}\big((c_tT^2N + c_sTN^2)D\big), \qquad \text{Memory} \sim \mathcal{O}\big(c_tT^2N + c_sTN^2\big),$$

while for the Full Attention baseline it is

$$\text{Compute} \sim \mathcal{O}\big(c_j(TN)^2D\big), \qquad \text{Memory} \sim \mathcal{O}\big(c_j(TN)^2\big).$$

Since the total depth is fixed, the overall complexity of the full network is linear in the number of units, and we omit this multiplicative factor for clarity. The resulting per-unit complexities for all nine PredFormer variants are summarized in Table 9.

Normalization of attention blocks. In our default configuration, we keep the number of *spatio-temporal units* the same for all variants, and each unit follows a specific ordering of temporal (T) and spatial (S) self-attention. For example, on Human3.6m, the Quadruplet-TSST variant is instantiated as `TSST`×3, which uses the same number of units as the Full Attention baseline; the only difference is that each unit in Quadruplet-TSST splits the attention into separate temporal and spatial operations, whereas the Full Attention baseline applies a joint self-attention over all TN tokens. This design ensures that our factorized variants do not gain an unfair advantage by simply reducing depth; instead, the observed differences in FLOPs, memory, and empirical performance can be attributed to the factorization pattern itself.

A.4 Experiment Setting

We provide our hyperparameter setting in Tab 10. For Moving MNIST, we use 24 GTB blocks for all PredFormer variants, which means 6 Quadruplet-TSST layers, 8 Triplet-TST layers, and 12 Binary-TS layers, respectively. For the TaxiBJ and WeatherBench datasets, we use 6 GTB blocks for the Triplet variants and 8 GTB blocks for the other variants.

Table 10: Hyperparameter Setting.

Hyperparameter	Moving MNIST	TaxiBJ	WeatherBench	Human3.6m
Training Hyperparameter				
Batch Size	16	16	16	8
Learning Rate	1e-3	1e-3	5e-4	{5e-4, 1e-3}
Learning Scheduler	Onecycle	Onecycle	Cosine	Cosine
Optimizer	Adamw	Adamw	Adamw	Adamw
Weight Decay	1e-2	1e-2	1e-2	1e-2
Training Epochs	2000	200	50	50
Model Hyperparameter				
Patch Size	8	4	4	8
GTB Blocks	24	{6,8}	{6,8}	12
GTB Dim	256	256	256	256
GTB Heads	8	8	8	8
SwiGLU Hidden Dim	1024	1024	512	1024
Attention Dropout	0.0	0.1	0.1	0.1
SwiGLU Dropout	0.0	0.1	0.1	0.1
Drop Path Rate	0.0	0.1	0.25	0.1

A.5 More Experiments

A.5.1 Comparison with Recent Recurrent Architectures

Tables 11 and 12 compare PredFormer with two recent recurrent architectures, SwinLSTM and VMRNN, on the Moving MNIST and TaxiBJ datasets, respectively. Across both benchmarks, PredFormer achieves lower MSE and higher SSIM while using comparable or fewer parameters and FLOPs. At the same time, PredFormer provides substantially faster training (shorter epoch time) and higher inference throughput (FPS), highlighting a favorable trade-off between accuracy and efficiency compared to these recurrent designs.

Table 11: Comparisons of PredFormer, SwinLSTM, and VMRNN on the Moving MNIST dataset.

Method	Paras (M)	Flops (G)	Epoch Time	MSE	SSIM
SwinLSTM	20.2	69.9	9min	17.7	0.962
VMRNN	–	–	18min	16.5	0.965
PredFormer 3TSST Layer	12.7	8.3	**1.5min**	16.2	0.965
PredFormer 6TSST Layer	25.3	16.5	3.5min	**12.5**	**0.973**

Table 12: Comparison of PredFormer, SwinLSTM, and VMRNN on the TaxiBJ dataset.

Method	Paras (M)	Flops (G)	Epoch Time	FPS	MSE	MAE	SSIM
SwinLSTM	2.9	1.3	–	1425	0.303	15.0	0.9843
VMRNN	**2.6**	**0.9**	5min	526	0.289	14.7	0.9858
PredFormer	6.3	1.6	**1min**	**2354**	**0.277**	**14.3**	**0.9864**

A.5.2 Ablation on Patch Size

To further analyze the effect of patch size, we fix the architecture to the Triplet-TST variant of PredFormer and vary the patch size from 8 to 4 on Moving MNIST. As shown in Table 13, using a smaller patch size (4×4) increases the number of spatial tokens from $N = 64$ to $N = 256$, which leads to higher computational cost (FLOPs 67.6G vs. 16.4G) and lower throughput (FPS 110 vs. 165). This finer granularity yields only a modest improvement in prediction accuracy (MSE 11.9 vs. 13.4, MAE 42.0 vs. 47.2, SSIM 0.974 vs. 0.971). Since the Triplet-TST variant with patch size 8 already outperforms all recurrent and convolutional baselines by a clear margin, we adopt patch size 8 as the default setting in the main experiments to achieve a better balance between accuracy and efficiency.

A.6 More Visualizations

Fig 7(a) and (b) depict the inflow and outflow at the same time step. In this case, the fourth frame shows significantly less traffic flow than the previous frames. Constrained by the inductive bias of CNNs, TAU continues to predict high traffic levels while PredFormer demonstrates superior generalization by accurately

Table 13: Patch size ablation of PredFormer (Triplet-TST) on **Moving MNIST** after training for **2000** epochs. Each model observes 10 frames and predicts the subsequent 10 frames with an input resolution of 64×64.

Patch Size	Resolution	Frames (in→out)	#Patches N	Variant	Paras(M)	Flops(G)	FPS	MSE ↓	MAE ↓	SSIM ↑
4	64×64	$10 \to 10$	256	Triplet-TST	25.3	67.6	110	11.9	42.0	0.974
8	64×64	$10 \to 10$	64	Triplet-TST	25.3	16.4	165	13.4	47.2	0.971

Table 14: Dataset characteristics and optimal PredFormer variants. P denotes patch size, T is the input temporal length, N is the number of spatial tokens after patch embedding, and N/T measures the spatial–temporal token ratio. The "Best Variant(s)" and "Best MSE" are taken from the main results tables under the default hyperparameters.

Dataset	Resolution ($H \times W$)	Patch Size P	#Patches N	T	N/T Ratio	Best Variant(s)	Best MSE ↓
Moving MNIST	64×64	8	$8 \times 8 = 64$	10	6	Quadruplet-TSST, Quadruplet-STTS	12.4
Human3.6m	256×256	8	$32 \times 32 = 1024$	4	256	Quadruplet-TSST	110.9
TaxiBJ	32×32	4	$8 \times 8 = 64$	4	16	Binary-ST, Triplet-STS	0.277
WeatherBench	32×64	4	$8 \times 16 = 128$	12	11	Fac-T-S	1.100

capturing this abrupt change. This capability highlights PredFormer's potential to handle extreme cases, which could be particularly valuable in applications like traffic flow prediction and weather forecasting.

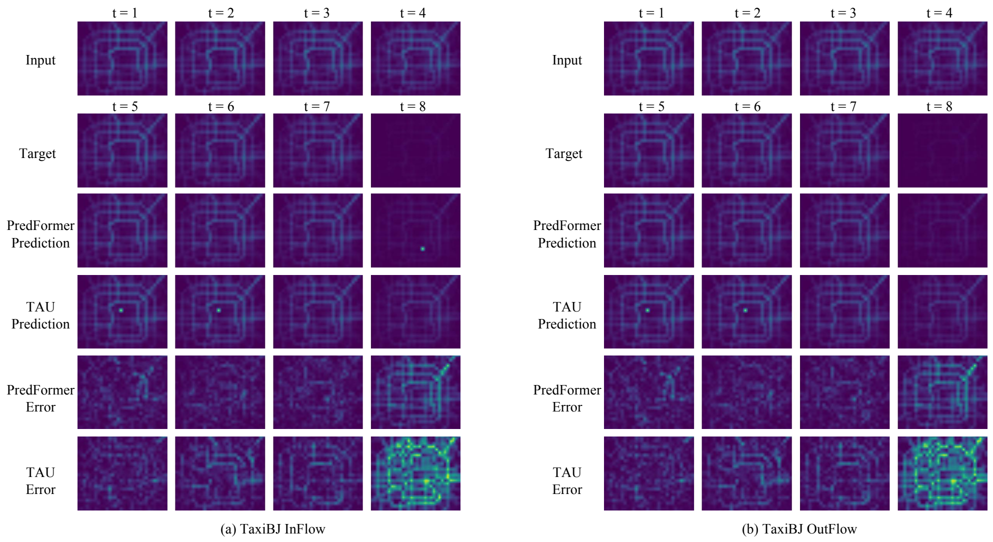

Figure 7: Visualizations on TaxiBJ InFlow and OutFlow. We amplify the error for better comparison.

A.7 Empirical Discussion on Optimal PredFormer Variants Across Tasks

To better understand why different PredFormer variants become optimal on different benchmarks, we summarize in Table 14 the key spatio-temporal characteristics of each dataset together with the best-performing PredFormer variant(s). As shown in Table 14, all four benchmarks favor factorized variants of PredFormer rather than the full-attention baseline, but the specific optimal pattern is dataset-dependent:

On WeatherBench, the temporal horizon is the longest ($T = 12$) while the spatial fields are relatively smooth. In this setting, the Fac-T-S variant, which applies temporal attention before spatial attention, performs best, suggesting that emphasizing temporal modeling early is beneficial for long-range geophysical forecasting.

On Human3.6m, the temporal window is short ($T = 4$), but the spatial resolution is very high (256×256 with $N/T = 256$), and human motion tightly couples spatial joints and temporal evolution. Here, the Quadruplet-

TSST variant, which interleaves two temporal and two spatial attention stages, works best, indicating that this dataset benefits from a balanced treatment of temporal and spatial dependencies.

On TaxiBJ, the temporal horizon is also short ($T = 4$), but the spatial grid is relatively low-resolution (32×32, $N/T = 16$) and dominated by structured traffic-flow patterns. In this regime, variants that allocate more capacity to spatial modeling at the end of the block (Binary-ST and Triplet-STS) perform best, suggesting that refining spatial correlations is especially important.

On Moving MNIST, both quadruplet variants (TSST and STTS) achieve the best results under the default patch size $P = 8$, indicating that a balanced four-stage factorization is robust on this synthetic but relatively long-horizon ($T = 10$) benchmark.

Overall, these results indicate that different spatio-temporal regimes (temporal horizon, spatial resolution, and the N/T ratio) naturally favor different factorization patterns within PredFormer, which explains why the optimal variant is not universal but dataset-specific.

A.8 Theoretical Analysis on PredFormer Variants' Performance Differences

We consistently observe that TSST outperforms TS, which in turn outperforms TST on datasets such as Moving MNIST, TaxiBJ, and Human3.6M. An exception occurs in WeatherBench, where this trend diverges due to severe overfitting. To analyze this phenomenon, we examine the representational capacity of temporal-first interleaved models. Unlike prior work that performs spatial-temporal attention factorization with a shared MLP, our approach allocates a dedicated SwiGLU FFN to each spatial and temporal attention block, enhancing the model's learning capacity and expressiveness. Then, the PredFormer encoder can be viewed as a spatial-temporal transformer sequence (e.g., TSSTTSST). We propose that a key factor influencing model performance is the number of unique spatial-temporal subsequence (e.g., TS, TST, TSST) partitions enabled by a given sequence. Sequences with richer and more diverse partition patterns are better able to capture complex spatio-temporal dependencies. We formalize this intuition through a unique partition counting algorithm, as described in Fig 8, and report the corresponding statistics in Tab 15. Notably, the number of unique partitions correlates well with empirical performance across configurations, offering a plausible explanation for the effectiveness of TSST.

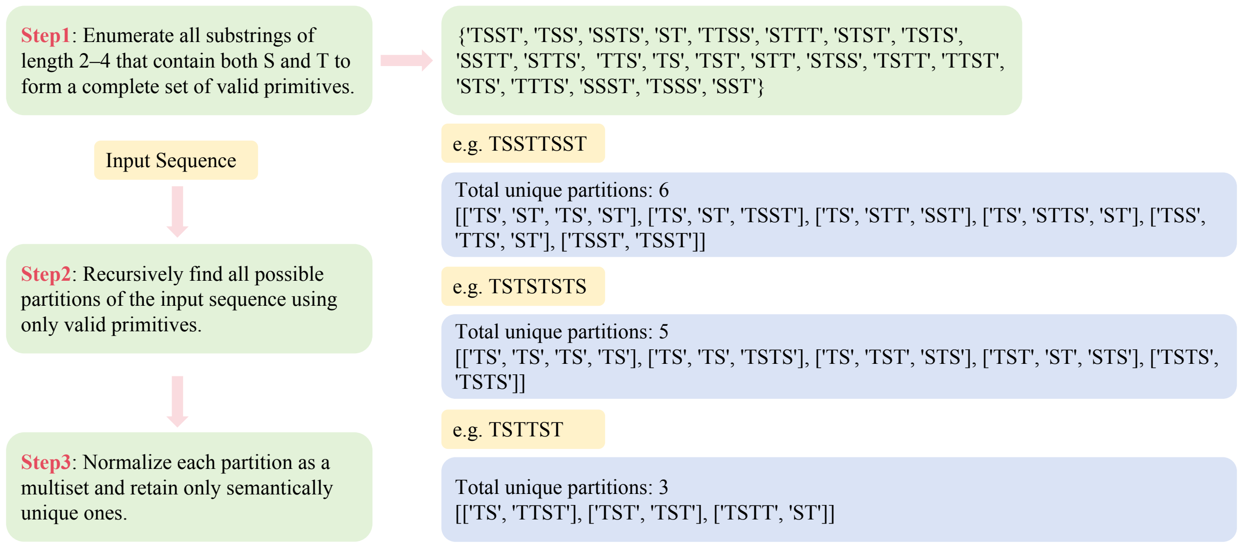
Step1: Enumerate all substrings of length 2–4 that contain both S and T to form a complete set of valid primitives.

{'TSST', 'TSS', 'SSTS', 'ST', 'TTSS', 'STTT', 'STST', 'TSTS', 'SSTT', 'STTS', 'TTS', 'TS', 'TST', 'STT', 'STSS', 'TSTT', 'TTST', 'STS', 'TTTS', 'SSST', 'TSSS', 'SST'}

Input Sequence

Step2: Recursively find all possible partitions of the input sequence using only valid primitives.

Step3: Normalize each partition as a multiset and retain only semantically unique ones.

e.g. TSSTTSST

Total unique partitions: 6
[['TS', 'ST', 'TS', 'ST'], ['TS', 'ST', 'TSST'], ['TS', 'STT', 'SST'], ['TS', 'STTS', 'ST'], ['TSS', 'TTS', 'ST'], ['TSST', 'TSST']]

e.g. TSTSTSTS

Total unique partitions: 5
[['TS', 'TS', 'TS', 'TS'], ['TS', 'TS', 'TSTS'], ['TS', 'TST', 'STS'], ['TST', 'ST', 'STS'], ['TSTS', 'TSTS']]

e.g. TSTTST

Total unique partitions: 3
[['TS', 'TTST'], ['TST', 'TST'], ['TSTT', 'ST']]

Figure 8: Spatial-Temporal GTB Unique Partition Algorithm.

Table 15: Analysis of Unique Partition Numbers.

Moving MNIST			Human3.6m			TaxiBJ		
Seq	Num ↑	MSE ↓	Seq	Num ↑	MSE ↓	Seq	Num ↑	MSE ↓
TSST*6	**160**	**12.4**	TSST*3	**16**	**110.9**	TSST*2	**6**	0.284
TS*12	116	12.8	TS*6	13	111.2	TS*4	5	**0.283**
TST*8	94	13.4	TST*4	11	112.4	TST*2	3	0.293